SCIENTIFIC NOTEBOOK

786E

by

Kwai S. Chan

Southwest Research Institute
Center for Nuclear Waste Regulatory Analyses
San Antonio, Texas

INITIAL ENTRIES

Scientific Notebook: #786E

Issued to: K.S. Chan

Issue Date: April 17, 2006

Account Number: 20.06002.01.222

Title: ~~Radionuclide Release Rates & Solubility Limits~~ Delayed Hydride Cracking of Cladding ECP 5/19/2011

Objective: To review, assess and evaluate the current status on the understanding of the potential role of delayed hydride cracking in the integrity of zirconium alloy cladding in high burnup nuclear fuel rods in the new TAD canisters.

June 1, 2006

Summarized current status of cladding stress from literature

Cladding Stresses:

Condition	Average Hoop Stress, MPa	Maximum Hoop Stress, MPa	Relaxed Hoop Stress, MPa	Cladding Temperature, C	Reference
Normal Reactor Operation (PWR, BWR)	24-62	134	N.A	320	Pescatore et al. 1989 [1]
Power Ramp		480			Ranjan et al. [2]
Power Ramp		520 -630	350-450	350-380	Schaffler et al. 2000 [3]
Power Ramp	280	350	210	350	Brochard et al. 2001 [4]
Power Ramp		300-400	N.A.	N.A.	Retel et al., 2004 [5]
Dry Storage	150 100			400 (initial) 220 (final)	Rashid and Machiels, 2005 [6]
Transport Accident				220	
Repository	60-100			< 320 (design) < 240 (average)	Siegmann [7] Ahn et al [8]

References:

1. C. Pescatore, M.G. Cowgill, anmd T.M.Sullivan, Zircaloy Cladding Performance Under Spent Fuel Disposal Conditions, Progress Report, may-1-October 31, 1989, BNL-52235, Upton, New York, Brookhaven National Laboratory. TIC Catalog Number: 224493.

2. G.V.Ranhan, G.N.Brooks, and A.K.Miller, Stresses and strains at Zircaloy cladding Ridges, Paper # D3/3, Transactions of SMIRT 5, Berlin, Germany,

3. I, Schaffler, P. Geyer, P. Bouffioux, and P. Delobelle, Thermomechnail behavior and modeling between 350C and 400C of Zircaloy-4 cladding tubes from an unirradiated state to high fluence, Journal of Engineering Materials and Technology, 2000, vol 122, pp. 168-176.

4. J. Brochard, F. Bentejac, N. Hourdequin, S. Seror, C. Verdeau, O. Fandeur, S. Lansiart, P. Verpeaux, Modeliing of Pellet cladding interaction in PWR fuel, Paper # 1314, Transactions of SMIRT 16, Washington DC, August 2001.

5. V. Retel, F. Trivaudey, M.L. Boubakar, D. Perreux, and P. Thevenin, Comparative effects of structural and material parameters variability on pellel-caldding interaction in a PWR fuel rod, Nuclear Engineering and design, 2004, vol 228, pp. 35-46.

6. J.Y.R. Rashid and A.J.Machiels, A methodology for the evaluation of fuel rod failures under accident conditions, RAMTRANS, 2005, vol. 16, No.3, pp. 211-218.

7. E. Siegmann, Cladding credits in TSPA-VA, Workshop on Alternative Models and Interpretations-Waste Form Degradation and Radionuclide Mobilization Expert Elicitation Project, San Francisco, CA, 1997.

8. T.M. Ahn, G.A. Cragnolino, K.S. Chan, and N. Sridhar, Scientific bases for cladding credit as a barrier to radionuclide release at the proposed YUCCA Mountain Repository, Mat. Res. Soc. Symp. Proc., Vol 556, 1999, pp. 525 –533.

June 9, 2006

DHC failure-time calculation at various stress levels

Pressure = 5 MPa; Temperature = 318.5C; K_{ox}=2.6 MPa(m)$^{1/2}$

K_{IH} = 5 MPa(m)$^{1/2}$

Input File	**Output File**	**Stress, MPa**	**K MPa(m)$^{1/2}$**	**T_f, hr**	**Reamrk**
Zrcrk-17.dek	Zrcrk-17.dat	400	8.708	6.051	Checked
Zrcrk-22.dek	Zrcrk-22.dat	350	7.630	6.086	Checked
Zrcrk-23.dek	Zrcrk-23.dat	300	6.551	7.218	Checked
Zrcrk-24.dek	Zrcrk-24.dat	290	6.335	7.466	Checked
Zrcrk-25.dek	Zrcrk-25.dat	280	---	---	No Oxide cracking
Zrcrk-26.dek	Zrcrk-26.dat	275	---	---	No Oxide cracking
Zrcrk-27.dek	Zrcrk-27.dat	285	6.227	7.608	Checked
Zrcrk-28.dek	Zrcrk-28.dat	282	6.161	7.678	Checked
Zrcrk-29.dek	Zrcrk-29.dat	275	6.012	7.891	Reduced K_{ox} to 1 MPa(m)$^{1/2}$
Zrcrk-30.dek	Zrcrk-30.dat	200	4.308	Infinity	No DHC
Zrcrk-31.dek	Zrcrk-31.dat	250	5.472	8.669	Checked
Zrcrk-32.dek	Zrcrk-32.dat	225	4.837	Infinity	No DHC
Zrcrk-33.dek	Zrcrk-33.dat	235	5.149	9.20	Checked
Zrcrk-34.dek	Zrcrk-34.dat	230	4.943	Infinity	No DHC

Files are in DIV 20 Cladding folders on Kwai Chan's desktop.

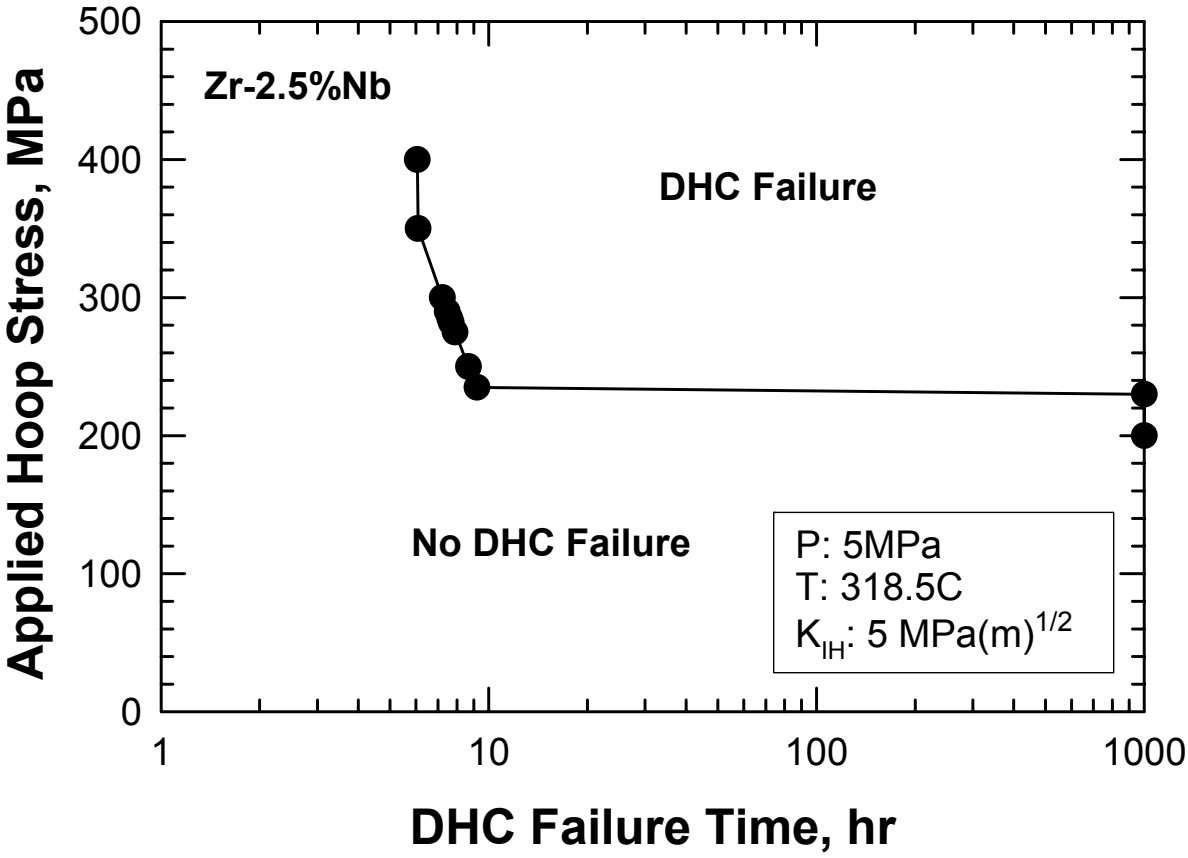

Figure 1. Computed DHC fialure times at various applied strss levels in the zirconium alloy cladding for K_{IH} = 5 MPa(m)½.

June 12, 2006

K_{IH} = 6 MPa(m)$^{1/2}$

Input File	Output File	Stress, MPa	K MPa(m)$^{1/2}$	T_f, hr	Remark
Zrcrk-35.dek	Zrcrk-35.dat	400	8.708	6.051	Checked
Zrcrk-36.dek	Zrcrk-36.dat	350	7.630	6.086	Checked
Zrcrk-37.dek	Zrcrk-37.dat	285	6.227	7.608	Checked
Zrcrk-38.dek	Zrcrk-38.dat	280	6.120	7.749	Checked

Zrcrk-39.dek	Zrcrk-39.dat	279	5.98	Infinity	No DHC
Zrcrk-40.dek	Zrcrk-40.dat	279.5	5.99	Infinity	No DHC

June 19, 2006

K_{IH} = 7 MPa(m)$^{1/2}$

Input File	Output File	Stress, MPa	K MPa(m)$^{1/2}$	T_f, hr	Remark
Zrcrk-41.dek	Zrcrk-41.dat	350	7.630	6.086	Checked
Zrcrk-42.dek	Zrcrk-42.dat	340	7.414	6.298	Checked
Zrcrk-43.dek	Zrcrk-43.dat	330	7.198	6.511	Checked
Zrcrk-44.dek	Zrcrk-44.dat	325	6.953	Infinity	No DHC
Zrcrk-45dek	Zrcrk-45dat	328	7.155	6.546	Checked
Zrcrk-46dek	Zrcrk-46dat	390	8.493	6.051	Checked

June 20, 2006

K_{IH} = 6 Mpa(m)^{½}

Varied a_i and b_i; a_i=b_i; Stress =300 MPa; Pressure = 5 Mpa

Delayed Hydride Cracking from Outer Wall and Inner Wall

Results fro Inner Wall Cracks

Input File	Output File	a_i =b_i, m	K MPa(m)$^{1/2}$	T_f, hr	Remark
Zrcrk-47.dek	Zrcrk-47.dat	1.0e-3	7.94	6.929	Checked
Zrcrk-48.dek	Zrcrk-48.dat	7.5e-4	6.83	7.202	Checked
Zrcrk-49.dek	Zrcrk-49.dat	5.0e-4	5.12	Infinity	No DHC

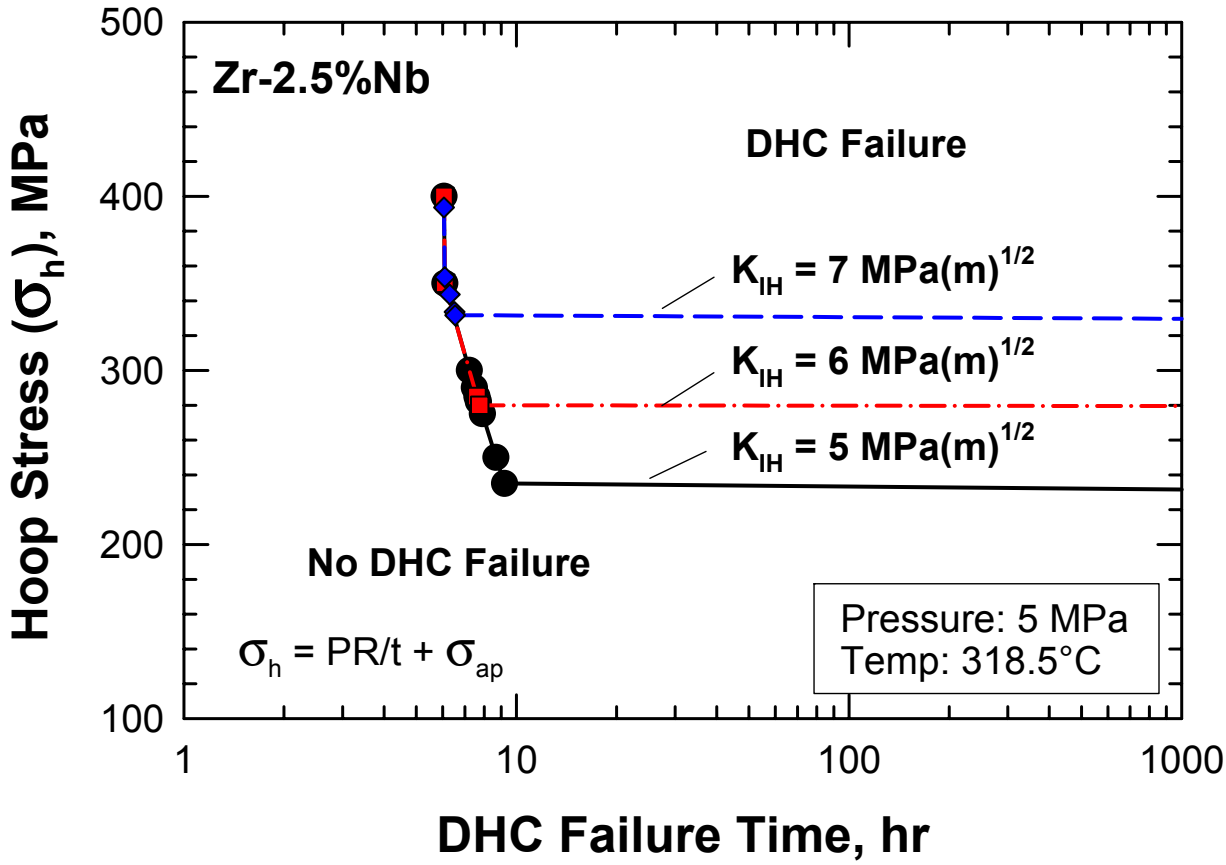

Figure 2. Computed stress-failure time curves for Zr-2.5% Nb with various K_{IH} values. P is pressure, R is radius, t is wall thickness of cladding tube, σ_h is the hoop stress, and σ_{ap} is the applied stress

K_{IH} = 6 Mpa(m)^{½}

Varied a_i and b_i; a_i=b_i=1.0e-4 m; varied stresses; pressure = 5Mpa

Check DHC of Inner-Wall Cracks

Input File	Output File	Stress, MPa	K MPa(m)$^{1/2}$	T_f, hr	Remark
Zrcrk-50.dek	Zrcrk-50.dat	300	2.27	Infinity	No DHC
Zrcrk-51.dek	Zrcrk-51.dat	400	3.26	Infinity	No DHC
Zrcrk-52.dek	Zrcrk-52.dat	500	3.78	Infinity	No DHC
Zrcrk-53.dek	Zrcrk-53.dat	600	4.53	Infinity	No DHC

K_{IH} = 5 Mpa(m)^{½}

Varied a_i and b_i; a_i=b_i; varied stresses; pressure = 5Mpa

Check DHC of Inner-Wall Cracks

Input File	Output File	Stress, Mpa a_i, m	K MPa(m)$^{1/2}$	T_f, hr	Remark
Zrcrk-54.dek	Zrcrk-54.dat	300;3.0e-4	3.95	Infinity	No DHC
Zrcrk-55.dek	Zrcrk-55.dat	300;4.0e-4	4.57	Infinity	No DHC
Zrcrk-56.dek	Zrcrk-56.dat	600;1.0e-4	4.53	Infinity	No DHC
Zrcrk-57.dek	Zrcrk-57.dat	600;5.0e-4	11.03	6.382	DHC
Zrcrk-58.dek	Zrcrk-58.dat	600;1.5e-4	6.00	6.801	DHC
Zrcrk-59.dek	Zrcrk-59.dat	600;1.2e-4	4.958	Infinity	No DHC
Zrcrk-60.dek	Zrcrk-60.dat	600;1.25e-4	5.479	6.838	DHC

Input and output files are stored in Div 20 Cladding folder/ZRCRACK sub-directory on Kwai Chan's desktop computer.

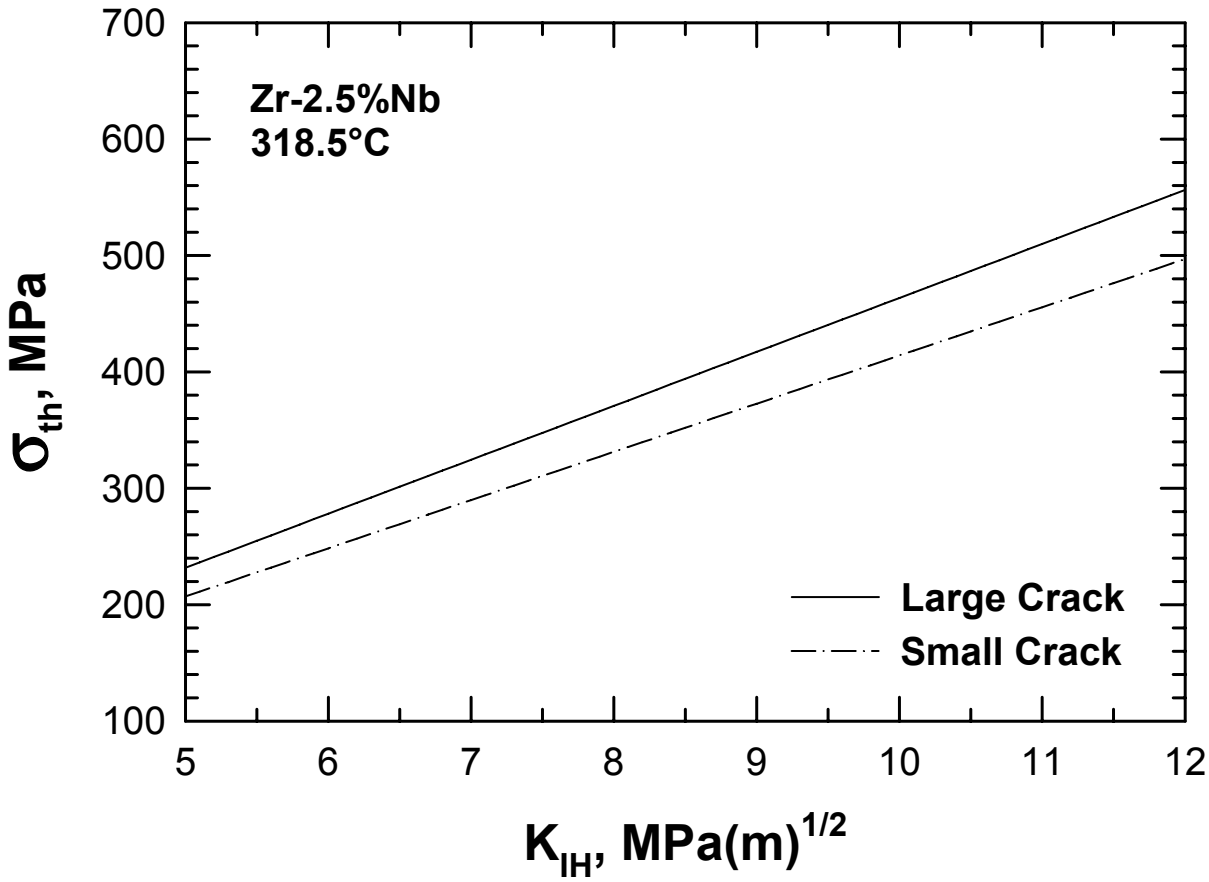

Figure 3. Computed threshold stress for DHC of large and small cracks in Zr-2.5% Nb as a function of K_{IH}.

June 21, 2006

Met with Tae Ahn from NRC and Yi-ming Pan to discuss delayed hydride cracking in cladding in TAD canister. Topics discussed included: (1) locals trains due to swelling can be as large as thermal expansion, (2) experimental observations of actual bonding of UO2 and cladding, and (3) ASTM symposium on hydride embrittlement is being planned for January 2007.

August 1, 2006

Delayed Hydride Cracking Under a Temperature Cooldown

DHC velocity

$$V = V_0 \exp\left[-\frac{Q_{DHC}}{RT}\right] \quad (1)$$ (Simpson and Puls) 1979

where V = crack velocity $= \frac{da}{dt}$

da = crack length increment

dt = time increment

V_0 = constant

Q_{DHC} = activation energy for delayed hydride crack

R = universal gas constant

T = absolute temperature

Eq (1) can be rewritten as

$$\frac{da}{dt} = V_0 \exp\left[-\frac{Q_{DHC}}{RT}\right] \quad (2)$$

leading to

$$da = v_0 \exp\left[-\frac{Q_{DHC}}{RT}\right] dt \qquad (3)$$

In addition

$$dt = \frac{dT}{\dot{T}} \qquad (4)$$

where $\dot{T}$ is the cooling rate

dT is the temperature change

substituting Eq (4) into Eq (3) gives

$$da = v_0 \exp\left[-\frac{Q_{DHC}}{RT}\right] \frac{dT}{\dot{T}} \qquad (5)$$

Integrating Eq (5) gives

$$\int_{a_1}^{a_2} da = \int_{T_1}^{T_2} \frac{v_0}{\dot{T}} \exp\left[-\frac{Q_{DHC}}{RT}\right] dT \qquad (6)$$

for a cooling from T_1 to T_2 with crack length changing from a_1 to a_2.

leading to

$$\Delta a = a_2 - a_1 = \sum_{T_n = T_1}^{T_n = T_2} \frac{V_0}{\dot{T}_n} \exp\left[-\frac{Q_{DHC}}{RT_n}\right] \Delta T_n \quad (7)$$

$$\Delta a = \sum_{T_n = T_1}^{T_n = T_2} \frac{V_0}{\dot{T}_n} \exp\left[-\frac{Q_{DHC}}{RT_n}\right] \Delta T_n \quad (8)$$

Calculations –

$\Delta T_n = 1°C$ ($1°K$)

$\dot{T}_n$ = constant (prescribed) (0.1 °C/s , 0.01 °C/s , and 0.001 °C/s)

$V_0 = 0.14$ m/s (20. R9565 Third Quarterly Report)

$Q_{DHC} = 65.5$ kJ/mol °K

Let $$X(T_n) = \frac{V_0}{\dot{T}_n} \exp\left[-\frac{Q_{DHC}}{RT_n}\right] \quad (9)$$

$$\Delta a = \sum_{T_n = T_1}^{T_n = T_2} X(T_n)\, \Delta T_n \quad (10)$$

where Δa is the DHC extension during the time increment of $\frac{\Delta T_n}{\dot{T}}$

August 4, 2006

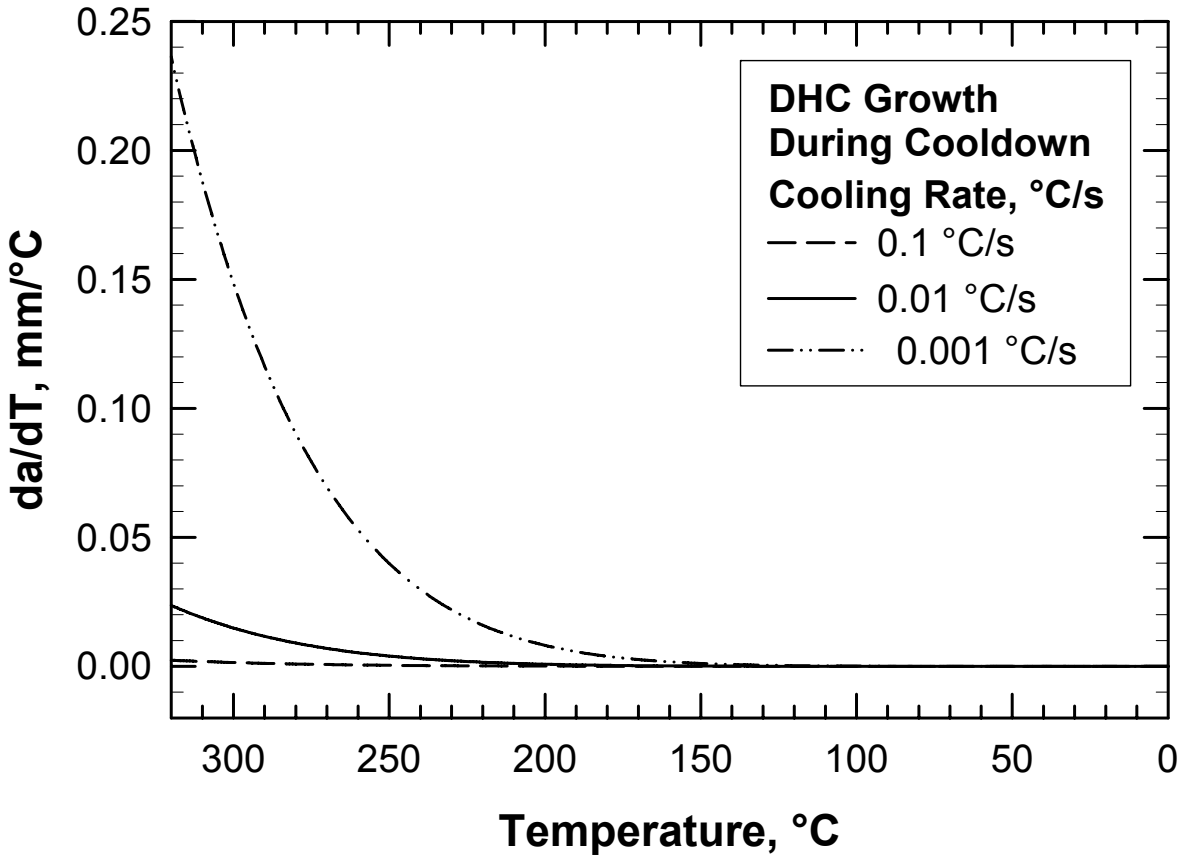

Figure 4. Computed da/dT as a function of temperature for three cooling rates.

The above analysis (dated August 1, 2006) was extended further to include DHC limited by hydride precipitation kinetics. For DHC under a cooldown from a give temperature, T (e.g., 320˚C), the crack extension per unit temperature change, dT, can be derived from Eq. (1) and is given by

$$\frac{da}{dT} = \frac{V_o}{\dot{T}} \exp\left[\frac{-Q_{DHC}}{RT}\right] \qquad \text{for T < 590K} \qquad (11)$$

and

$$\frac{da}{dT} = \frac{V_o^h}{\dot{T}} \exp\left[\frac{Q_h}{RT}\right]$$

for T < 590K (12), where $\dot{T}$ is the cooling rate; T_1 and T_2 are the initial and final temperatures in the cooldown cycle. The importance of the cooling rate on the DHC growth response is illustrated in Figure 5, which shows a plot of da/dT as a function of temperature for three different cooling rates for Zr-2.5%Nb with Vo=0.14 m/s, R=8.321 J/mol, and Q_{DHC} = 65.5 kJ/mol/K for T < 317˚C where hydride precipitation is controlled by diffusion kinetics. For T > 317˚C where hydrogen solubility controls hydride precipitation, V_o^h = 8.83E-42 m/s and Q_h = 389 kJ/mol. Figure 5 shows that the amount of DHC growth per temperature change is highest at about 317˚C and deceases with decreasing temperatures for all three cooling rates. DHC growth is essentially non-existent when the temperature is above 360˚C because hydrogen is in solid solution and hydrides cannot be formed at the crack tip. DHC growth is very limited when the temperature drops below 150˚C because of slow diffusion kinetics. A high cooling rate reduces the DHC growth because there is less time for the crack to propagate

during the prescribed cooling rate. Conversely, a slow cooling rate allows more time for DHC to occur.

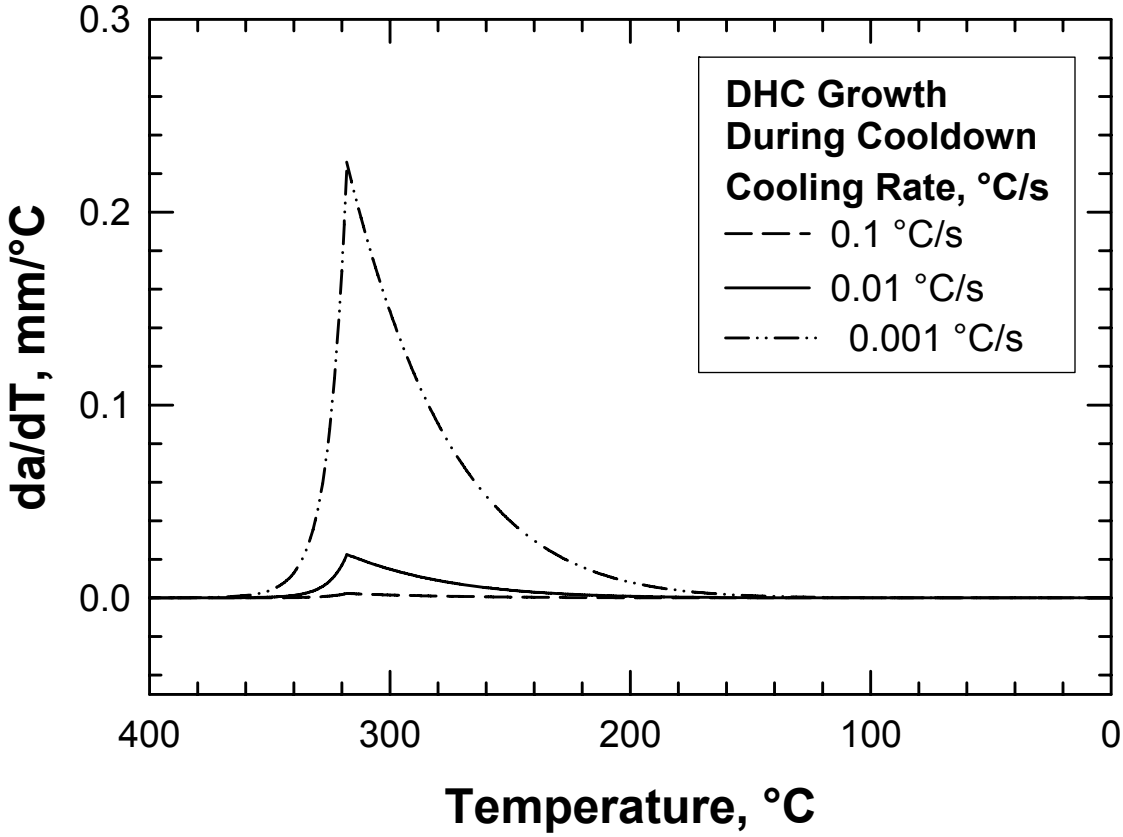

Figure 5. DHC growth rate per unit temperature change as a function of cladding temperature for three cooling rates.

The cumulative crack extension by DHC during the cooldown is given by the area under the curves shown in Figure 5 and is obtained by integrating or summing Eqs. (11 and 12) over the temperature range from T_1 to T_2, leading to

$$\Delta a = \int_{T_1}^{T_2} \frac{V_o}{\dot{T}} \exp\left(\frac{-Q_{DHC}}{RT} \right) dT + \int_{T_2}^{T_3} \frac{V_o^h}{\dot{T}} \exp\left(\frac{Q_h}{RT} \right) dT \tag{13}$$

and the results for cooling from T_3 =400 to T_1 = 0˚C with T_2 = 317˚C are summarized in Table 1 for the three cooling rates.

Table 1. DHC Crack Extensions and Time of Growth as a Function of Cooling Rates

Cooling Rate, ˚C/s	**Δa , mm ($T_3 \rightarrow T_2$)**	**Δa , mm ($T_2 \rightarrow T_1$)**	**Δa , mm ($T_3 \rightarrow T_1$)**	**Time (hrs)**
0.1	0.0109	0.0889	0.0998	1.11
0.01	0.1807	0.8888	1.0695	11.11
0.001	1.8075	8.8876	10.695	111.11

Table 1 shows that the amount of DHC extension is about 0.1mm for a cooling rate of 0.1 C/s and the time spent in DHC growth is 1.1 hours. When the cooling rate is reduced to 0.01 C/s, the time available for DHC growth increases to 11.11 hours and the amount of DHC extension increases to 1.07 mm. Further decrease in the cooling rate to 0.001 C/s increases the DHC time to 111 hours and the amount of DHC extension to 10.7 mm. Since the cladding wall-thickness is typically about 6 mm, DHC growth has penetrated the wall-thickness after 62 hours at this slow cooling rate. The results suggest that there is sufficient time for delayed hydride cracking to cause complete cladding failure if it takes more than 2 ½ days to cool the cladding rods from 320˚C to below 25˚C.

August 18, 2006

The time, t_h, required for the diffusion of hydrogen to from hydrides at a crack tip can be estimated from the expression given by

$$t_h = \frac{l_h^2}{4D_h} \tag{14}$$

with

$$D_h(m^2/s) = 2.17x10^{-1}\exp\left(-\frac{8380}{RT}\right) \tag{15}$$

where l_h is the distance must diffuse to reach the crack tip to form hydrides, R is the universal gas, T is absolute temperature, and D_h is the diffusion coefficient of hydrogen in zirconium. Using Eqs. (20) and (21), the times required for diffusion distances of 20, 100, and 1000 μm are computed and the results are shown as a function of temperature in Figure 25. For all three diffusion distances, the times for diffusion of hydrogen to the crack tip are small compared the stress transient in power ramp, which is on the order of 10 minutes or higher. Thus, there are sufficient times for the diffusion of hydrogen to the crack tip to form hydrides. For impact loading due to transport accidents, the time requirement may be met at least for the 20 and 100 μm cases, if not for all three cases. For seismic loading, the stress transient may be on the order a microsecond. Under this circumstance, the stress

transient due to seismic loading might be too short for diffusion of hydrogen to the crack tip to hydrides.

The high transient stresses associated with impact and seismic loading can potentially cause crack initiation in cladding by fracturing a hydride blister and a number of radial hydrides. Once a crack of sufficient depth is formed, the stress due to the internal gas pressure might then be large enough to cause subsequent DHC growth. If not, DHC growth would cease and remain dormant until the crack is activated again by a subsequent transient stress cycle.

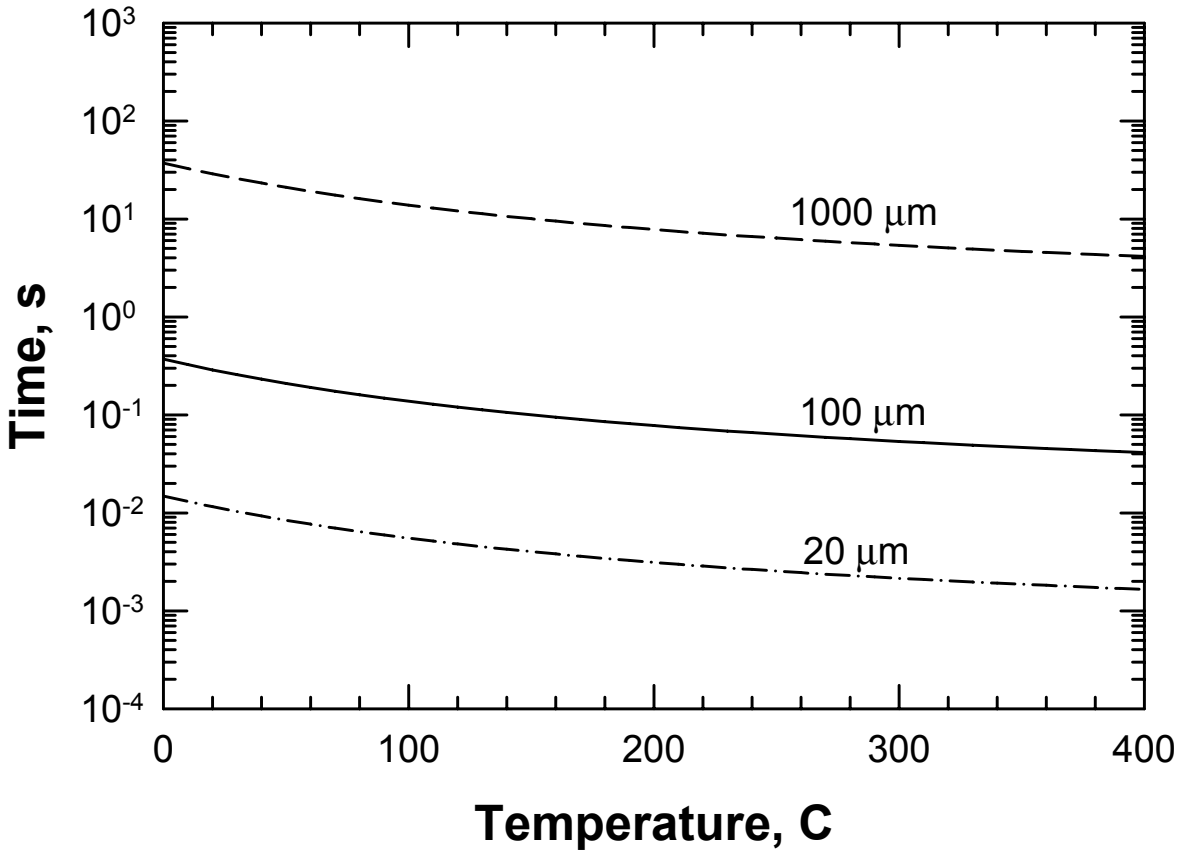

Figure 6. Times required for the diffusion of hydrogen atoms from various distance to form hydrides at the crack tip.

August 22, 2006

The growth threshold for small crack, K_{IH}^{SC}, and large crack, K_{IH}^{LC}, are related according to the expression given by (Chan et al, 2001)

$$K_{IH}^{SC} = K_{IH}^{LC}\sqrt{\frac{a}{a + a_o}} \tag{16}$$

where a is crack length and a_o is the small cracl parameter. The value of a_o can be computed on the basis of the fracture stress corresponds to the hydride fracture strength, σ_f^h and the large crack threshold, K_{IH}^{LC} at a = a_o using linear-elastic fracture mechanics, leading to

$$a_o = \frac{1}{\pi}\left[\frac{K_{IH}^{LC}}{F\sigma_f^h}\right] \tag{17}$$

where F is crack geometry correction factor with F = 1.12 for an edge crack with a shallow crack depth (e.g., a/W < 0.05) . Using the appropriate a_o for various K_{IH} values at 300 and 600K, Eq, (16) was utilized to predict the K_{IH} values for small cracks as a function of crack length and the results are presented in Figure 7. The result shows that the K_{IH} value for small cracks in zirconium alloys approaches to a very small value at diminishing crack size. On the other hand, hydride fracture occurs only the hydride length exceeds a critical length.

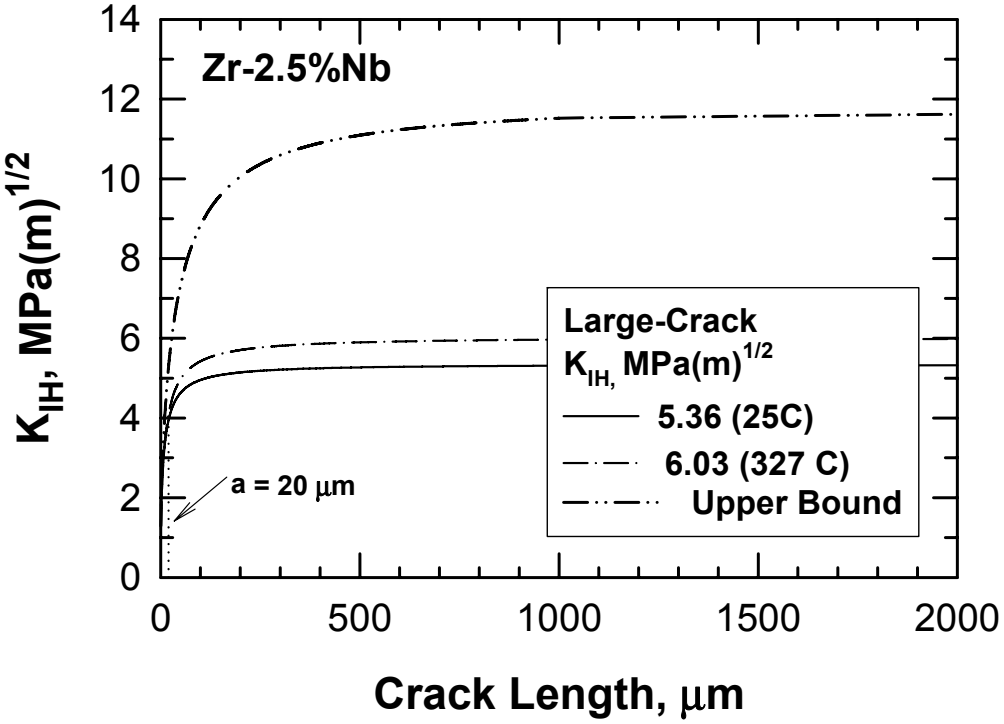

Figure 7. Dependece of K_{IH} growth threshold on crack length. The K_{IH} value is about 4 MPa(m)$^{1/2}$ at a = 20 μm but it increases rapidly with increasing crack length.

The fracture stresses for large cracks and small cracks propagated by DHC were computed and compared as a function of crack length in Figure 8. The hydride fracture stress data are from Shi and Puls (1999). F=0.86 for semi-circular cracks. Small crack model is based on Eq. (16). Large crack model is based on large-crack K_{IH} value.

Shi, S.Q. and M.P. Puls. "Fracture Strength of Hydride Precipitates in Zr-2.5Nb Alloys." *Journal of Nuclear Materials.* Vol. 275. pp. 312-317. 1999.

August 25, 2006

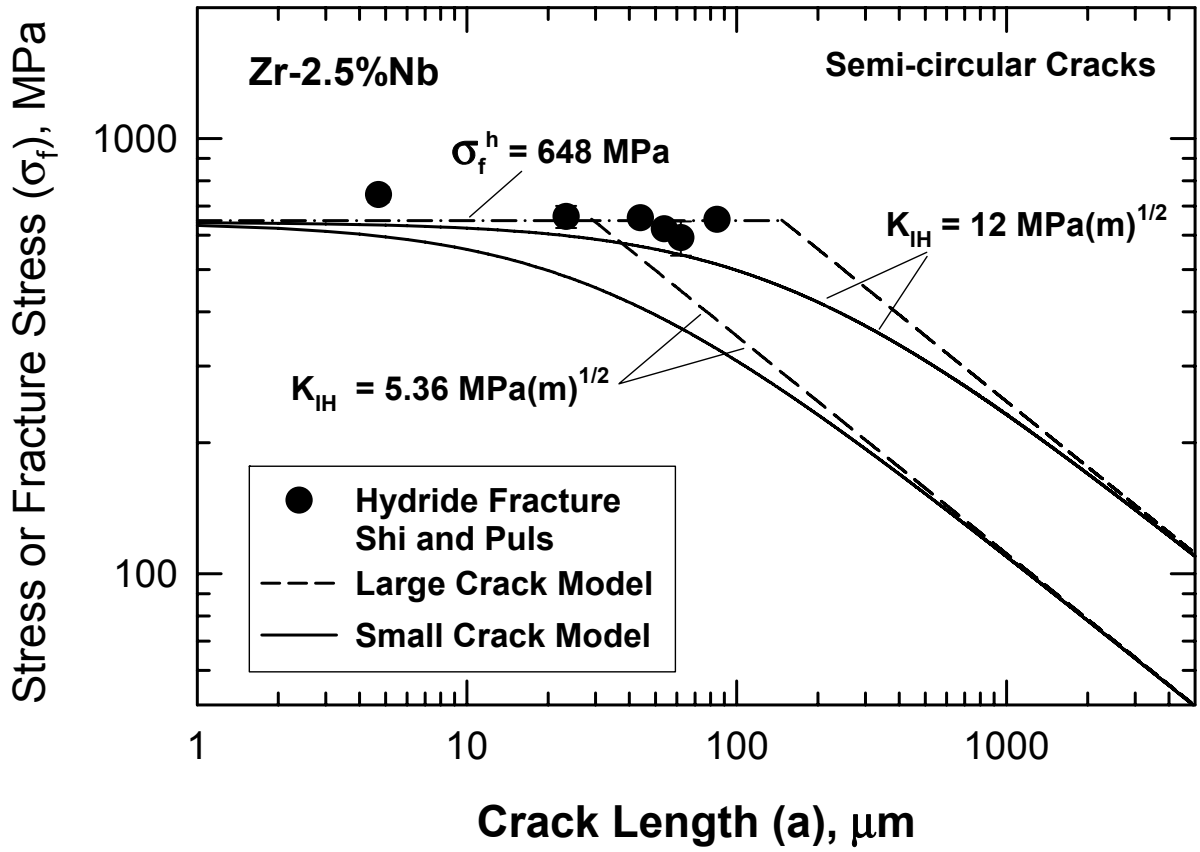

Figure 8. Plot of stress or fracture stress for delayed hydride cracking as a fucntion of crack length.

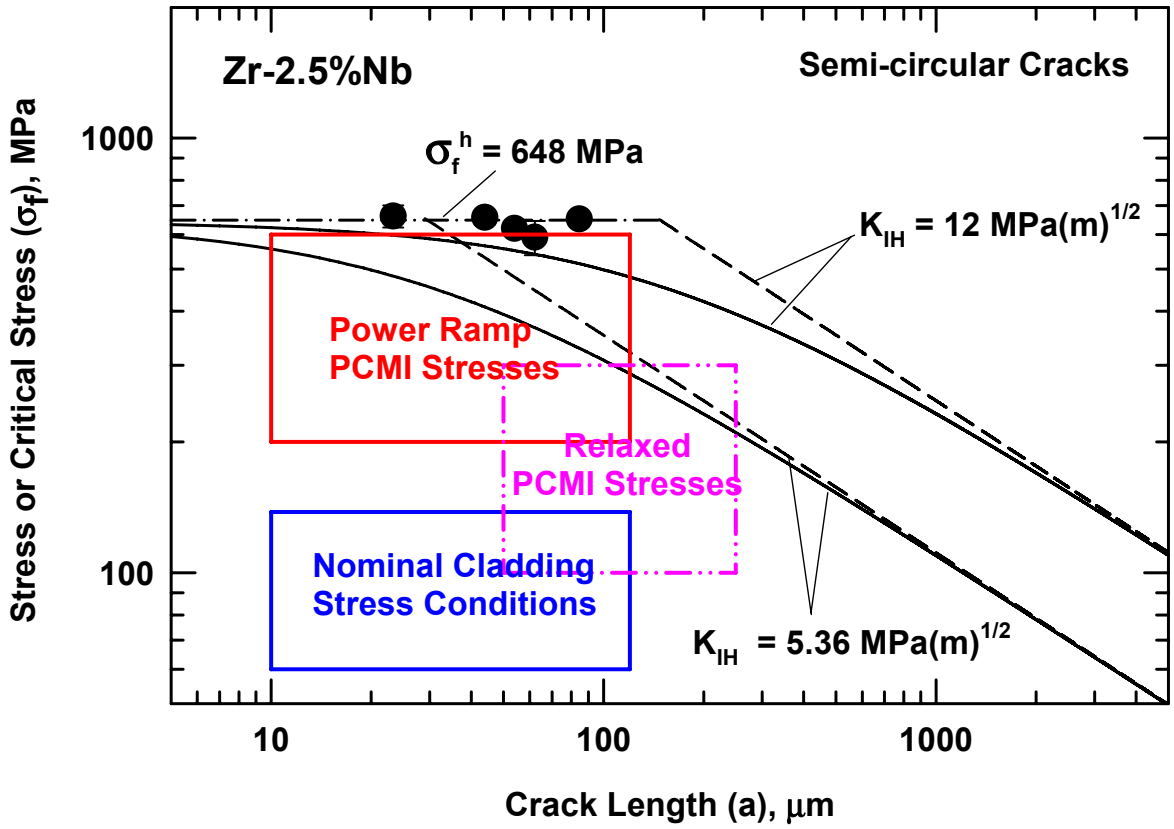

Figure 9. A comparison of cladding stresses under various loading conditions and crack lengths against the large-crack and small-crack threshold stresses for the onset of delayed hydride cracking in Zr-alloy cladding tubes

Nominal cladding stress: 60 -120 MPa, crack length: 10-120 mm

Data are from

CRWMS M&O. "Initial Cladding Condition." ANL-EBS-MD-000048. Rev. 00 ICN 01. Las Vegas, Nevada: CRWMS M&O. 2000.

Cladding stress transeints during power ramps: 200 -600 MPa and 10 – 120 μm crack length.

Relaxed stresses: 100 - 300 Mpa; 50 – 250 μm crack length (based on intial crack elngth + dHC during power ramps).

Unrelaxed and relaxed Power ramp transient hoop stresses are from Brochard et al. (1997, 2001), Suzuki and Uetsuka (2002), and Schäffler et al. (2000)

Brochard, J., F. Bentejac, and N. Hourdequin. "Nonlinear Finite Element Studies of the Pellet-Cladding Mechanical Interaction in a PWR Fuel." Transactions of the Fourteenth International Conferences on Structural Mechanics in Reactor Technology (SMiRT 14), Lyon, France, August 17-22, 1997. Paper CW/4, pp. 271-278. 1997.

Brochard, J., F. Bentejac, N. Hourdequin, S. Seror, C. Verdeau, O. Fandeur, S. Lansiart, and P. Verpeaux. "Modelling of Pellet Cladding Interaction in PWR Fuel." Transactions of the Sixteenth International Conferences on Structural Mechanics in Reactor Technology (SMiRT 16), Washington DC, USA, August, 2001. Paper No. 1314, pp. 1-8. 2001.

Schäffler, I., P. Geyer, P. Bouffioux, and P. Delobello. "Thermomechancial Behavior and Modeling Between 350˚C and 400˚C of Zircaloy-4 Cladding Tubes from an Unirradiated State to High Fluence (0 to 85 x 10^{24} nm^{-2}, E > 1MeV)." *Journal of Engineering Materials and Technology.* Vol. 122. pp. 169-176. 2000.

Suzuki, M. and H. Uetsuka. "Development of Fuel Performance Code FEMAXI-6 and Analysis of Mechanical Loading on Cladding During Power Ramp for High Burn-Up Fuel Rod." Fuel Failure in Water Reactors: Causes and Mitigation. Proceedings of a Technical Meeting held in Bratislava, Slovakia, June 17-21, 2002. IAEA-TECDOC-1345. pp. 217-238. 2003.

ADDITIONAL INFORMATION FOR SCIENTIFIC NOTEBOOK NO. 786E

Document Date:	06/01/2006
Availability:	Southwest Research Institute® Center for Nuclear Waste Regulatory Analyses 6220 Culebra Road San Antonio, Texas 78228
Contact:	Southwest Research Institute® Center for Nuclear Waste Regulatory Analyses 6220 Culebra Road San Antonio, TX 78228-5166 Attn.: Director of Administration 210.522.5054
Data Sensitivity:	■"Non-Sensitive" □ Sensitive □"Non-Sensitive - Copyright" □ Sensitive - Copyright
Date Generated:	04/12/2011
Operating System: (including version number)	Windows
Application Used: (including version number)	
Media Type: (CDs, 3 ½, 5 1/4 disks, etc.)	1 CD
File Types: (.exe, .bat, .zip, etc.)	dek, dat, zrcrk
Remarks: (computer runs, etc.)	Notebook supplemental material